Multi-Physics Inversion of Acoustic and Electromagnetic Wave Fields

Ramirez, Ana B.; De Wit, Anne V.; Van Dongen, Koen W.A.

DOI
10.1109/LAUS60931.2024.10553197

Publication date
2024

Document Version
Final published version

Published in
Proceedinsg of the IEEE UFFC Latin America Ultrasonics Symposium, LAUS 2024

Multi-physics Inversion of Acoustic and Electromagnetic Wave fields

Ana B. Ramirez
Dept. of Electrical and Electronics Engineering
Industrial University of Santander
Bucaramanga, Colombia
anaberam@uis.edu.co

Anne V. de Wit
Department of Imaging Physics
Delft University of Technology
Delft, the Netherlands
anneveradewit@gmail.com

Koen W.A. van Dongen
Department of Imaging Physics
Delft University of Technology
Delft, the Netherlands
k.w.a.vandongen@tudelft.nl

2024 IEEE UFFC Latin America Ultrasonics Symposium (LAUS) | 979-8-3503-4908-5/24/$31.00 ©2024 IEEE | DOI: 10.1109/LAUS60931.2024.10553197

***Abstract*—Multi-modality or multi-physics imaging is gaining interest beacuase it overcomes the limitations of a single imaging modality, as each modality typically suffers from its own application specific limitations. Different imaging techniques are developed to combine the outcome of both modalities; varying from image fusion up to the usage of prior information obtained from one imaging modality and used as input for the other one. In this work an alternative approach is presented. The method employs a multi-physics Born inversion algorithm where structural similarity is used as regularization parameter to align the acoustic and electromagnetic contrast interfaces with each other. To align the interfaces the gradients of the acoustic and electromagnetic contrast functions are used. Two approaches are tested successfully on a synthetic profile; one where the cross-product of the two gradients and one where the gradient differences are considered. Both approaches work but the gradient-difference approach outperforms the cross-gradient one. Overall, it is shown that multi-physics Born inversion both approaches reveals details in the electromagnetic contrast function that would have been missed by only employing electromagnetic inversion. This improvement is obtained at the cost of an increase in computational complexity compared to single modality inversion.**

***Index Terms*—multi-physics inversion, multi-modality, joint inversion, Born, acoustic, electromagnetics**

I. Introduction

Acoustic and electromagnetic waves are both used separately for breast cancer detection. [1]–[3] Recently, multi-modality or multi-physics imaging is gaining interest from the medical as well as the geophysical society. [4]–[7] Mainly, as it overcomes the limitations of a single imaging modality, as each modality typically suffers from its own application specific limitations. Different imaging techniques are developed to combine the outcome of both modalities, varying from image fusion up to the usage of prior information obtained from one imaging modality and used as input for the other one. [5]–[7]

In this work an alternative multi-physics imaging method is presented. The new method combines both acoustic and electromagnetic measurements during the inversion. A multi-modality imaging systems typically consists of acoustic and electromagnetic sources and receivers located on a surface $\mathbb{S}$ in a homogeneous embedding with constant speed of sound and speed of light. The surface $\mathbb{S}$ encloses the spatial domain of interest $\mathbb{D}$ that shows contrasts in the acoustic and electromagnetic medium properties, see Fig. 1. Although the amplitudes of the acoustic and electromagnetic contrast may be different, they have in common that their interfaces are at the same location. During the reconstruction of the acoustic and electromagnetic medium properties this prior knowledge is taken to our advantage and included as an extra constraint in the inversion scheme. This work is a continuation of the work done by Ozdemir where only the gradient difference between the acoustic and electromagnetic contrast was considered. [4]

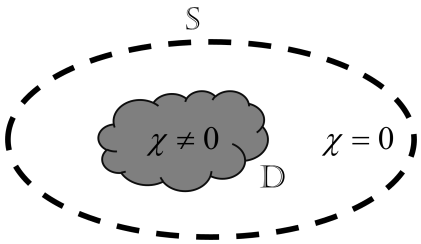

Fig. 1. Schematic representation of a multi-modality imaging system. The region of interest $\mathbb{D}$ shows contrast in the acoustic (χ_A) and dielectric medium properties (χ_E) and is enclosed by a collection of acoustic and electromagnetic transceivers located on a surface $\mathbb{S}$ in a domain with zero contrast ($\chi_A = \chi_E = 0$).

To test our method, we first present the theory in section II Theory. In section III Methods, the employed configuration is shown as well as the tested contrast profiles. Section IV Results shows the outcome of our method for the tested contrast profiles. Section V present the discussion and conclusion.

II. Theory

A. Acoustic wave fields

The two-dimensional acoustic pressure wave field $p(\boldsymbol{x}, t)$ at the location $\boldsymbol{x} = (x, y)$ and time instant t is governed by the scalar wave equation [8]

$$\nabla^2 p(\boldsymbol{x}, t) - \frac{1}{c_A^2(\boldsymbol{x})} \frac{\partial^2 p(\boldsymbol{x}, t)}{\partial t^2} = -S_A(\boldsymbol{x}, t), \tag{1}$$

where $c_A(\boldsymbol{x})$ is a spatially varying speed-of-sound profile and $S_A(\boldsymbol{x}, t)$ the primary acoustic source.

Equation (1) may be recast into an integral equation of the second kind that reads [8]

$$\hat{p}(\boldsymbol{x}) = \hat{p}^{\mathrm{inc}}(\boldsymbol{x}) + \hat{p}^{\mathrm{sct}}(\boldsymbol{x}), \tag{2}$$

where $\hat{p}^{\mathrm{inc}}(\boldsymbol{x})$ denotes the incident field in the temporal Fourier domain. Here the caret symbol $\hat{}$ is used to denote that a given quantity is defined in the temporal Fourier domain with angular frequency ω. The incident field is obtained via convolution of the primary source $\hat{S}(\boldsymbol{x})$ with the Green's function $\hat{G}_A(\boldsymbol{x}-\boldsymbol{x}')$, i.e. the impulse response of the homogeneous embedding, hence

$$\hat{p}^{\mathrm{inc}}(\boldsymbol{x}) = \int_{\boldsymbol{x}'\in\mathbb{S}} \hat{G}_A(\boldsymbol{x}-\boldsymbol{x}')\hat{S}_A(\boldsymbol{x}')\mathrm{dS}(\boldsymbol{x}'). \tag{3}$$

For the 2-D case of interest, the Green's function $\hat{G}_A(\boldsymbol{x}-\boldsymbol{x}')$ is based on Hankel functions of the first kind, therefore

$$\hat{G}_A(\boldsymbol{x}-\boldsymbol{x}') = \frac{-i}{4}H_0^{(1)}(\omega\left|\boldsymbol{x}-\boldsymbol{x}'\right|/c_{A;0}), \tag{4}$$

with $c_{A;0}$ the speed of sound of the embedding. The scattered field denoted by $\hat{p}^{\mathrm{sct}}(\boldsymbol{x})$ equals within the Born approximation [9]

$$\hat{p}^{\mathrm{sct}}(\boldsymbol{x}) = \frac{\omega^2}{c_{A;0}^2}\int_{\boldsymbol{x}'\in\mathbb{D}} \hat{G}_A(\boldsymbol{x}-\boldsymbol{x}')\chi_A(\boldsymbol{x}')\hat{p}^{\mathrm{inc}}(\boldsymbol{x}')\mathrm{dS}(\boldsymbol{x}'), \tag{5}$$

with acoustic contrast function $\chi_A(\boldsymbol{x}')$

$$\chi_A(\boldsymbol{x}') = \frac{c_{A;0}^2}{c_A^2(\boldsymbol{x}')} - 1, \tag{6}$$

with $c_A(\boldsymbol{x}')$ the speed of sound of the actual medium.

B. Electromagnetic wave fields

Similar to the acoustic case, the propagation of the electric wave field $\hat{\boldsymbol{E}}(\boldsymbol{x})$ in heterogeneous media may be described using integral equations as well. For the electric field, and in particular for the transverse magnetic (TM) case, the resulting integral equation reads [8]

$$\hat{\boldsymbol{E}}(\boldsymbol{x}) = \hat{\boldsymbol{E}}^{\mathrm{inc}}(\boldsymbol{x}) + \hat{\boldsymbol{E}}^{\mathrm{sct}}(\boldsymbol{x}) \tag{7}$$

where the incident electric field $\hat{\boldsymbol{E}}^{\mathrm{inc}}(\boldsymbol{x})$ is generated by a free electric current $\hat{\boldsymbol{J}}(\boldsymbol{x}')$ and equals

$$\hat{\boldsymbol{E}}^{\mathrm{inc}}(\boldsymbol{x}) = \int_{\boldsymbol{x}'\in\mathbb{S}} \hat{G}_E(\boldsymbol{x}-\boldsymbol{x}')\hat{\boldsymbol{J}}(\boldsymbol{x}')\mathrm{dS}(\boldsymbol{x}'), \tag{8}$$

where $\hat{G}_E$ is the electromagnetic Green's function, viz.

$$\hat{G}_E(\boldsymbol{x}-\boldsymbol{x}') = \frac{-i}{4}H_0^{(1)}(\omega\left|\boldsymbol{x}-\boldsymbol{x}'\right|/c_{E;0}), \tag{9}$$

with $c_{A;0}$ the speed of sound of the embedding. The scattered electric field $\hat{\boldsymbol{E}}^{\mathrm{sct}}(\boldsymbol{x})$ in equation (7) reads within the Born approximation

$$\hat{\boldsymbol{E}}^{\mathrm{sct}}(\boldsymbol{x}) = \frac{\omega^2}{c_{E;0}^2}\int_{\boldsymbol{x}'\in\mathbb{D}} \hat{G}_E(\boldsymbol{x}-\boldsymbol{x}')\chi_E(\boldsymbol{x}')\hat{\boldsymbol{E}}^{\mathrm{inc}}(\boldsymbol{x}')\mathrm{dS}(\boldsymbol{x}'), \tag{10}$$

where the electric contrast function $\chi_E(\boldsymbol{x}')$ is defined as

$$\chi_E(\boldsymbol{x}') = \frac{c_{E;0}^2}{c_E^2(\boldsymbol{x}')} - 1, \tag{11}$$

with $c_E(\boldsymbol{x}')$ the speed of light of the actual medium.

C. Joint inversion with structural similarity approach

Determining the unknown acoustic and electromagnetic contrast functions from the measured scattered field is in principle a non-linear ill-posed inverse problem. However, we for this particular test we linearized the inverse problem by employing the Born approximation. This means that we made the assumption that the contrast is small compared to the wave length of the probing wave field and/or that the contrast is weak. To reconstruct the acoustic and electromagnetic contrast functions, we employ a conjugate gradient scheme to minimize the following error functional [1]

$$F(\chi_A,\chi_E) = F_{\mathrm{Born}}(\chi_A,\chi_E) + F_{\mathrm{Struct}}(\chi_A,\chi_E). \tag{12}$$

The first term on the right-hand side of equation (12) accounts for the error in the computed wave fields based on the reconstructed contrast function, hence

$$F_{\mathrm{Born}}(\chi_A,\chi_E) = \frac{\parallel \hat{p}^{\mathrm{sct}} - \hat{G}_A\chi_A\hat{p}^{\mathrm{inc}} \parallel^2}{\parallel \hat{p}^{\mathrm{inc}} \parallel^2} + \frac{\parallel \hat{E}^{\mathrm{sct}} - \hat{G}_E\chi_E\hat{E}^{\mathrm{inc}} \parallel^2}{\parallel \hat{E}^{\mathrm{inc}} \parallel^2}. \tag{13}$$

The second term on the right-hand side of equation (12) accounts for the structural similarity using the gradients of the contrast functions. To accomplish this, we test two methods; one where we consider the gradient difference (GD), viz.

$$F_{\mathrm{Struct;GD}}(\chi_A,\chi_E) = \beta \parallel \nabla\chi_A - \nabla\chi_E \parallel^2, \tag{14}$$

and another where we consider cross gradient (CG), viz.

$$F_{\mathrm{Struct;CG}}(\chi_A,\chi_E) = \beta \parallel \nabla\chi_A \times \nabla\chi_E \parallel^2, \tag{15}$$

where β is a regularization parameter allowing us to weaken or strengthen the structural similarity constraint. [4]

III. Methods

To test the proposed method, we consider the setup shown in Fig. 2(a-b). Here, a circular scanning system encloses a circular contrast which on its turn encloses the characters TU. The system contains 16 acoustic/electromagnetic sources and 128 acoustic/electromagnetic receivers equally distributed on the circular array. For the acoustic measurements we consider a Gaussian pulse with a center frequency of 0.1 MHz and for the electromagnetic measurements a Gasussian pulse with a center frequency of 1 GHz. The corresponding center wavelengths are defined by $\lambda_{A;0} = 15$ mm and $\lambda_{E;0} = 225$ mm, indicating a significantly larger wavelength for the electromagnetic case. The spatial domain of interest is a squared region of 96 mm by 96 mm discretized into 64×64 cells.

Snapshots of the modeled wave fields including higher-order scattering are shown in Fig. 2. These are obtained by solving the full-wave problem using a conjugate gradient scheme. [9] The resulting wave fields are used as input for the Born inversion.

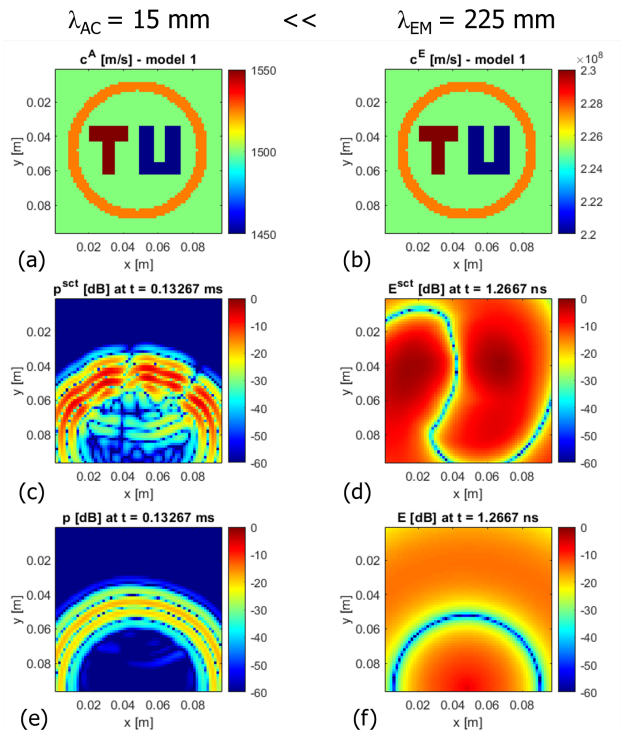

Fig. 2. The synthetic acoustic (a) and electromagnetic (b) models are tested separately. The resulting scattered wave fields (c-d) are used as input for the Born inversion. For completeness, also both total wavefields (e-f) are shown.

IV. Numerical Results

First we reconstruct the acoustics and electromagnetic contrasts separately, i.e. we take $\beta = 0$. The Born-inversion results are shown in Fig. 2(c) and Fig. 2(d). The obtained results clearly show that the acoustics contrast function is reconstructed quite accurately, whereas the reconstructed electromagnetic contrast function does not provide any detail at all. Next, a mask is employed. The mask ensures that it is only possible to reconstruct a contrast at the location of the synthetic profile. By employing this mask, it becomes feasible to reconstruct the amplitudes of the corresponding contrasts, see Fig. 3(e-f). It is known that by employing such a mask the inverse problem is simplified drastically. [10], [11]

Next, the cross-gradient method is applied with $\beta \approx 10^{-7}$. The aim is to improve the electromagnetic reconstruction by taking the acoustic reconstruction into account, see Fig. 2(g-h). It is clear that the use of the reconstructed acoustic contrast as an input for the inversion improves the resolution of the electromagnetic reconstruction. Finally, the gradient-difference approach is tested. The resulting reconstructions are shown in Fig. 2(i-j). This time, the improvement in the electromagnetic contrast function is even more significantly as compared to the cross-gradient based results.

V. Discussion and Conclusion

Acoustic and electromagnetic imaging modalities are frequently used as ”stand-alone” or single-modality imaging

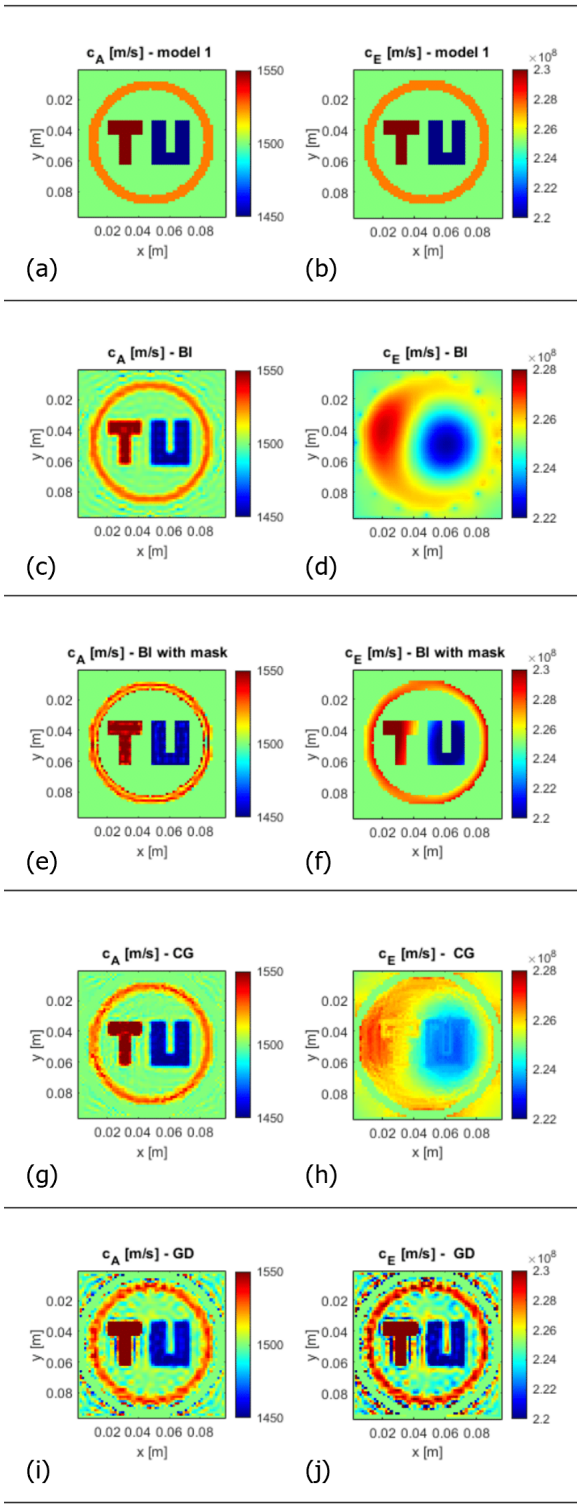

Fig. 3. The synthetic acoustic (a) and electromagnetic (b) models are first reconstructed separately yielding (c-d). Next, a mask is employed allowing us to reconstruct the contrast with great detail and nearly correct amplitudes as shown in (e-f). Finally two joint inversion methods are tested, first the cross-gradient method shown in (g-h) followed by the gradient-difference method shown in (i-j).

modalities for medical and seismic applications. Recently, multi-modality or multi-physics imaging is gaining interest as it may overcome the limitations of a single imaging modality, as each modality typically suffers from its own application specific limitations. Different imaging techniques are developed to combine the outcome of both modalities. In this work we test the approach of adding an additional regulazation term in our iterative inversion scheme. The additional regularization term is based on structural similarity and successfully couples the electromagnetic and acoustic contrast functions. It is observed that a coupling via the gradient-difference of the two contrast functions outperforms the approach of considering the cross-gradient as a regularization term.

Given the success of machine learning in combination with breast ultrasound [12], [13] it is worth to investigate if machine learning can also be used to link acoustic and electromagnetic medium properties with each other. Especially as there might be a link between the amplitudes of the acoustic and electromagnetic contrast functions for each tissue. Finally, the proposed multi-physics inversion methods may also be of interest for those working on multi-parameter inversion to reconstruct for mass density and compressibility simultaneously, which is of interest to both the medical and the seismic community. [14], [15]

To conclude, in this paper, we presented a multi-modality or multi-physics imaging algorithm to improve the resolution for ultrasound and electromagnetic imaging. The method uses structural similarity as additional constrained during inversion. This structural similarity may be included via gradient-difference or cross-gradient constraint. Our preliminary numerical results indicate that the gradient-difference approach outperforms the cross-gradient constraint.

ACKNOWLEDGMENTS

This work was partially supported by the Colombian Ministry of Science, Technology, and Innovation, under the grant No. 715 of 2022.

REFERENCES

[1] N. Ozmen, R. Dapp, M. Zapf, H. Gemmeke, N.V. Ruiter, and K.W.A. van Dongen, "Comparing different ultrasound imaging methods for breast cancer detection," IEEE Transactions on Ultrasonics, Ferroelectrics, and Frequency Control, vol. 62(4), pp. 637-646, April 2015.

[2] M.S.S. Alwan, and Z. Katbay "Investigation of tumor using an antenna scanning system," Proc. IEEE 2014 Mediterranean Microwave Symp., 2014.

[3] L.L. Wang, "Microwave Sensors for Breast Cancer Detection," Sensors, vol. 18(2), February 2018.

[4] O. Ozdemir, A. Oncu, and K.W.A. van Dongen, "A Joint Inversion Method for Breast Imaging using Electromagnetic and Acoustics waves," 20th International Conference on Electromagnetics in Advanced Applications (ICEAA 2018), 8th IEEE-APS Topical Conference on Antennas and Propagation in Wireless Communications (IEEE-APWC 2018), 14th lnternational Workshop on Finite Elements for Microwave Engineering (FEM 2018) (Cartagena de Indias, Colombia, September 10-14, 2018).

[5] X. Song, M. Li, F. Yang, S. Xu, and A. Abubakar, "Three-Dimensional Joint Inversion of EM and Acoustic Data Based on Contrast Source Inversion," in IEEE Journal on Multiscale and Multiphysics Computational Techniques, vol. 5, pp. 28-36, 2020.

[6] Z. Fang et al., "A Review of Emerging Electromagnetic-Acoustic Sensing Techniques for Healthcare Monitoring," in IEEE Transactions on Biomedical Circuits and Systems, vol. 16, no. 6, pp. 1075-1094, December 2022.

[7] M. Salucci, L. Poli, S. Lusa, Z. Lin, M. Li, and A. Massa, "Recent Advances in Multiscale-Multiphysics Inverse Scattering," 2024 18th European Conference on Antennas and Propagation (EuCAP), Glasgow, United Kingdom, 2024.

[8] A.T. de Hoop, Handbook of Radiation and Scattering of Waves. London, Academic Press, 1995.

[9] U. Taskin, N. Ozmen, H. Gemmeke, and K.W.A. van Dongen, "Modeling breast ultrasound; on the applicability of commonly made approximations," Archives of Acoustics 43(3), pp. 425-435, April 2018.

[10] K.W.A. van Dongen, C. Brennan, and W.M.D. Wright, "A reduced forward operator for acoustic scattering problems," IET Digital Library.

[11] K.W.A. Van Dongen, C. Brennan, and W.M.D. "Wright Reduced forward operator for electromagnetic wave scattering problems," IET Science, Measurement & Technology 1 (1), 57-62, January 2007.

[12] W. Zhao, H. Wang, H. Gemmeke, K.W.A. van Dongen, T. Hopp, and J. Hesser, "Ultrasound Transmission Tomography Image Reconstruction with Fully Convolutional Neural Network," Physics in Medicine & Biology 65 (23), 235021, November 2020.

[13] W. Zhao, Y. Fan, H. Wang, H. Gemmeke, K.W.A. van Dongen, T. Hopp, and J. Hesser, "Simulation-to-real generalization for deep-learning-based refraction-corrected ultrasound tomography image reconstruction," Physics in Medicine & Biology 68(3), 35016, 2023.

[14] U. Taskin, and K.W.A. van Dongen, "Multi-parameter inversion with the aid of particle velocity field reconstruction," Journal of the Acoustical Society of America 47(6), pp. 4032-4040, May 2020.

[15] M. Jakobsen, K. Xiang, and K.W.A. van Dongen, "Seismic and medical ultrasound imaging of velocity and density variations by nonlinear vectorial inverse scattering," The Journal of the Acoustical Society of America 153 (5), 3151-3151, 2023.